Optics Letters

Graphene-gold supercapacitor as a voltage controlled saturable absorber for femtosecond pulse generation

Isinsu Baylam,[1] Osman Balci,[2] Nurbek Kakenov,[2] Coskun Kocabas,[2] and Alphan Sennaroglu[1,*]

[1]*Laser Research Laboratory, Departments of Physics and Electrical-Electronics Engineering, Koç University, Istanbul 34450, Turkey*
[2]*Department of Physics, Bilkent University, Ankara 06800, Turkey*
Corresponding author: asennar@ku.edu.tr

We report, for the first time to the best of our knowledge, use of a graphene-gold supercapacitor as a voltage controlled fast saturable absorber for femtosecond pulse generation. The unique design involving only one graphene electrode lowers the insertion loss of the device, in comparison with capacitor designs with two graphene electrodes. Furthermore, use of the high-dielectric electrolyte allows reversible, adjustable control of the absorption level up to the visible region with low bias voltages of only a few volts (0–2 V). The fast saturable absorber action of the graphene-gold supercapacitor was demonstrated inside a multipass-cavity Cr:forsterite laser to generate nearly transform-limited, sub-100 fs pulses at a pulse repetition rate of 4.51 MHz at 1.24 μm. © 2016 Optical Society of America

In recent years, numerous unique optoelectronic properties of graphene have been demonstrated [1,2]. In particular, because of its ultrafast response [3] and nearly constant absorption over a very broad wavelength range [4], graphene has been shown to function as a fast saturable absorber for the generation of femtosecond pulses from a variety of lasers operating in the near- and mid-infrared [5–7]. However, one major drawback stems from the fact that even a mono-atomic layer of graphene introduces a small-signal round-trip loss of approximately 5% inside a laser resonator, causing a notable increase in lasing threshold and reduction in power efficiency, especially in low-gain bulk solid-state lasers such as Cr:forsterite and Cr:colquiriites. To overcome this problem, different approaches such as chemical or electrostatic doping have been recently proposed to vary the position of the Fermi level and to control the absorption level in graphene, while maintaining a sufficient level of saturable absorption to initiate mode locking [8,9]. The chemical doping of graphene layers causes an irreversible change in the Fermi

level position, and the shift cannot be dynamically controlled [9]. On the other hand, adjustable control of absorption can be achieved by using biased graphene-based solid-state or supercapacitor structures that use electrostatic doping to shift the Fermi level. In the case of solid-state graphene capacitors, operation is typically limited to infrared wavelengths, since modulation of absorption requires relatively high bias voltages at short wavelengths and may lead to dielectric breakdown [8,10]. In the case of a graphene-based supercapacitor, which was first reported as a voltage controlled saturable absorber by our groups, use of an organic electrolyte with a high-dielectric constant and the resulting formation of an ultrathin electric double layer (EDL) [11] at the graphene-electrolyte junction make it possible to shift the Fermi level with low bias voltages on the order of several volts, even in the visible region [12,13]. Such a graphene-based supercapacitor has been recently demonstrated by our groups as an effective saturable absorber to generate femtosecond pulses from a Cr:forsterite laser near 1250 nm [13]. The experimental results clearly indicated that the small-signal round-trip insertion loss of the device could be reduced while maintaining a sufficient modulation depth to initiate mode-locked operation. One drawback of the supercapacitor design of [13] was that both capacitor electrodes were made of graphene, giving an additional 5% insertion loss. These results suggest that the optimum graphene supercapacitor design for mode locking should include only one graphene electrode to minimize insertion losses and to maximize the efficiency of the mode-locked laser.

In this Letter, we demonstrate, for the first time to the best of our knowledge, the mode-locking performance of a novel graphene device based on a voltage controlled graphene-gold supercapacitor saturable absorber (VCG-gold-SA). The VCG-gold-SA is composed of an ionic liquid electrolyte sandwiched between graphene and gold electrodes. The mode-locking performance of the VCG-gold-SA was demonstrated inside a multipass-cavity Cr:forsterite laser operating near 1240 nm. Our experiments clearly showed that as the bias voltage of the VCG-gold-SA was increased, the overall absorption of the device could be reduced, and mode locking could be obtained

at lower pump powers. Furthermore, the VCG-gold-SA could be operated with lower insertion loss, in comparison with the previous supercapacitor design containing two graphene electrodes [13]. At a pump power of 4.66 W, nearly transform-limited, 80 fs, 3.3 nJ pulses were generated at 1240 nm. Figure 1(a) shows a sketch of the VCG-gold-SA, which consists of a room temperature ionic liquid electrolyte (diethymethyl (2-methox-yethyl) ammonium bis (trifluro- methylsulfony) imide [DEME] [TFSI]) between graphene and gold electrodes. The graphene electrode was synthesized by chemical vapor deposition (CVD) and transfer printed onto an infrared transparent (Infrasil) window. The gold electrode with a 5-mm diameter hole was fabricated with thermal evaporation. We used a 5 nm Ti adhesive layer under the gold layer. The hole at the center of the gold electrode was patterned by using shadow evaporation.

The electrical connections to the graphene and gold electrodes were made by using carbon tapes. Raman spectrum measurements of our CVD grown graphene electrode yielded the characteristic G and 2D bands at 1595 and 2688 cm^{-1}, respectively. The frequency of the 2D peak further indicated that the unintentional doping level resulted in a Fermi level shift of 0.2 eV [14]. The intensity ratio of the 2D to G peaks was around 1.7. The intensity of the defect peak was negligible, suggesting a low level of defects. The inset in Fig. 1(b) shows the small-signal circuit model of the VCG-gold-SA. The graphene electrode is modeled as a variable resistor (R_G^T) and variable capacitor whose capacitance (C_G) is given by the quantum capacitance (C_Q) of graphene:

$$C_Q = e^2 D = \frac{2e^2}{\hbar \nu_F} \sqrt{\frac{n}{\pi}}. \tag{1}$$

Here, D is the density of states, ν_F is the Fermi velocity (1.1×10^6 m/s), n is the effective carrier density, and $\hbar$ is the Planck's constant. Figure 1(b) shows the measured variation of the capacitance of the device as a function of the bias voltage at 20 Hz. The capacitance is minimum at the Dirac point (−0.5 V) and increases up to 2.7 µF/cm^2 at 2 V. Since the capacitance of the electrical double layer ($C_{EDL} \sim 30$ µF/cm^2) and surface capacitance of the gold electrode are much larger than the quantum capacitance of the graphene electrode, the equivalent capacitance of the device is mainly defined by the quantum capacitance of the graphene electrode. Note that our optical modulator is based on ionic gating. Unlike a dielectric capacitor where the voltage drops linearly through the
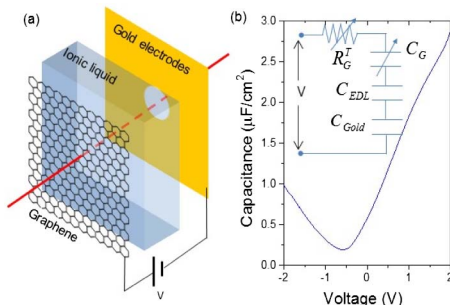
dielectric layer, for ionic gating, the electric field is generated within a very thin electrical double layer (EDL) which is a few nanometers thick. EDL is formed conformally on the graphene surface. The mobile ions of the electrolyte migrate until they screen the electric field on the graphene. The hole on the gold electrode and the thickness of the ionic liquid do not affect the formation of the EDL. The geometrical parameters only affect the time scale of EDL formation which is around 0.2 s for our device. Figure 2(a) shows the measured fractional change in the optical transmission spectrum of the VCG-gold-SA as a function of the bias voltage. Due to Pauli blocking, the VCG-gold-SA becomes transparent for photon energies smaller than twice the Fermi level shift, as shown in the inset of Fig. 2(b). By using this fact, the Fermi energy shift with respect to the Dirac point was determined as a function of the applied bias voltage [see Fig. 2(b)]. As shown in Fig. 2(b), the Fermi energy shift increases linearly with increasing bias voltage. When the gold layer was used as a gating electrode, the Fermi level shift at zero bias was 0.5 eV due to the mismatch of the work functions of graphene and gold electrodes.

To test the mode-locking performance of the VCG-gold-SA, a multi-pass cavity (MPC) laser architecture similar to that in [13] was used. In addition to the VCG-gold-SA, the resonator consisted of a Brewster-cut, 20 mm long Cr:forsterite crystal, MPC optics for cavity extension, and dispersion control optics. A schematic of the experimental setup is shown in Fig. 3. The Cr:forsterite crystal was end pumped with a Yb fiber laser at 1.064 µm and kept at 20.5°C. The resonator was extended with a q-preserving MPC which consisted of a curved (M5, $R = 4$ m) and a flat (M6) high reflector. Each MPC mirror had a notch for beam injection and extraction. To maintain the q-preserving condition, the distance between M5 and M6 was set to 165 cm, and the exiting beam was retro-reflected by another curved end mirror (M8, $R = 2$ m) located at a distance of 165 cm from M5 [15]. The pulse repetition rate of the composite cavity, including the original x-cavity, MPC, and the dispersion control optics, was 4.51 MHz. Together with the dispersion control mirrors (M1–M4, M7, and M9–M15 in Fig. 3), the net estimated group delay dispersion
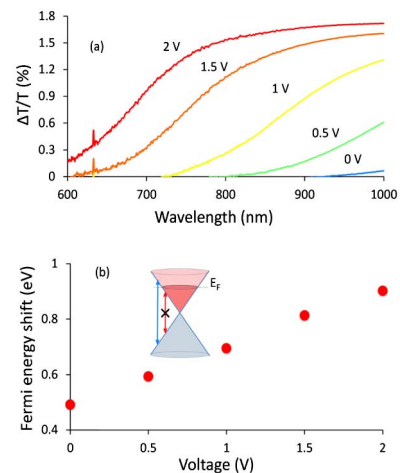

Fig. 1. (a) Schematic drawing of the graphene-gold supercapacitor used as a voltage controlled saturable absorber. (b) Variation of the capacitance of the device as a function of the bias voltage. The Dirac point is shifted by −0.5 V. The inset shows the small-signal circuit model of the device.

Fig. 2. (a) Measured fractional change in the optical transmission spectrum of the VCG-gold-SA as a function of the bias voltage (b) Estimated Fermi energy shift of the device as a function of the applied voltage.
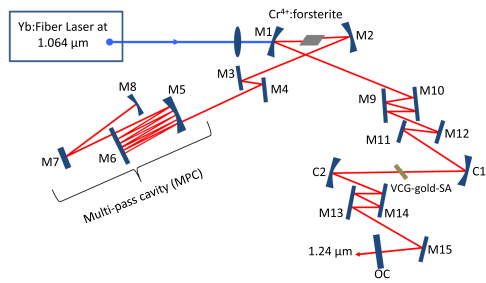
Fig. 3. Experimental setup of the multi-pass cavity Cr:forsterite laser used for testing the mode-locking performance of the VCG-gold-SA. The output coupler (OC) transmission was 2.4%.

(GDD) of the resonator was −4432 fs^2. The VCG-gold-SA was positioned between two curved high reflectors (C1 and C2, each with a radius of curvature 50 cm) at Brewster incidence to minimize reflection losses and eliminate etalon effects during mode-locked operation. The estimated beam waist on the VCG-gold-SA was 115 μm.

The continuous-wave power performance of the Cr:forsterite laser with different cavity configurations is shown in Fig. 4(a). Without the VCG-gold-SA, the threshold pump power and the slope efficiency for the short x-cavity with 4.7% output coupler (OC) were measured to be 1.8 W and 17.5%, respectively. The addition of MPC and dispersion compensation optics reduced the slope efficiency of the free running laser to 13% and increased the threshold pump power to 3 W. Without the VCG-gold-SA, the estimated single-pass insertion loss due to Cr:forsterite crystal, MPC, and dispersion compensation optics was determined to be 3.14%, 0.94%, and 2.5%, respectively. Because the small-signal insertion loss of the VCG-gold-SA was in excess of 5%, we were not able to operate the composite laser with 4.7% output coupler [16]. As a result, the mode-locking experiments were conducted with a 2.4% output coupler. With this output coupler, we obtained 16 mW of output power at the input pump power of 7.15 W before applying a bias voltage to the VCG-gold-SA. As Fig. 4(b) shows, by
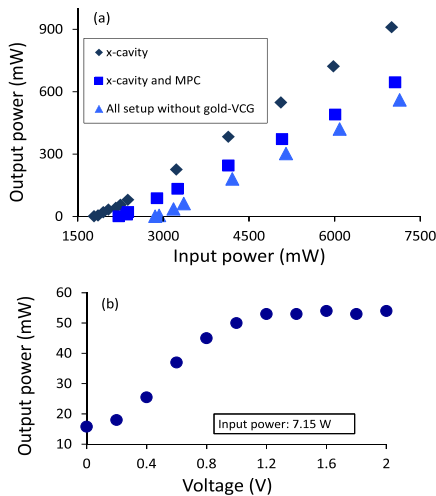
applying a bias voltage, the loss of the VCG-gold-SA could be reduced, and the output power could be increased. In particular, with a fixed input power of 7.15 W, the output power of the Cr:forsterite laser could be increased from 16 to 54 mW as the bias voltage was increased from 0 to 2 V.

To estimate the voltage dependent insertion loss of the VCG-gold-SA, we measured the threshold pump power of the composite Cr:forsterite laser at different bias voltages and deduced the effective loss of the VCG-gold-SA by assuming that the threshold pump power is proportional to $(L + T)$, where L is the total loss of the resonator, and T is the output coupler transmission [16]. In our case, $T = 2.4\%$ and $L = L_C + L_{SA}$, where L_C is due to the crystal, MPC; dispersion control optics is $(3.14 + 0.94 + 2.5) = 6.58\%$; and L_{SA} is the voltage-dependent roundtrip insertion loss of the VCG-gold-SA. Figure 5 shows the measured single-pass insertion loss of the VCG-gold-SA ($1/2\ L_{SA}$) and of our previous supercapacitor design containing two graphene electrodes (VCG-SA) [13]. The advantage of the graphene-gold design can be clearly seen from the data of Fig. 5. Note that, because approximately 0.8 V is needed per graphene layer to block absorption at 1240 nm, the device with a single graphene electrode reaches lower loss levels at noticeably lower operating voltages (in the 0–0.8 V range), in comparison with the previous design containing two graphene electrodes. Also note that lower insertion loss of the VCG-SA design at sufficiently large voltages is due to the use of substrates with higher optical quality, since at these voltages, graphene absorption is completely blocked.

For bias voltages between 0 and 0.8 V, single pulse mode-locked operation could be initiated at 1.24 μm by translating the output coupler. In our previous study [13], at pump powers at or below 7 W, mode-locked operation could not be observed for bias voltages below 0.5 V. Because the current design of the VCG-gold-SA reduced the optical insertion loss, mode locking could be obtained at lower bias voltages. Figure 6 shows that the measured mode-locking threshold pump power as a function of the applied bias. As the bias voltage was increased from 0 to 0.8 V, the mode-locking threshold pump power decreased from 7.15 to 5.14 W. At bias voltages above 0.8 V, the modulation depth of the graphene became insufficient to initiate saturable absorber action and no mode locking could be observed for the laser wavelength for voltages beyond 0.8 V. Note that since the mode-locking threshold pump power depends, among other factors, on the insertion loss of the VCG-gold-SA, it followed a similar trend as in Fig. 5 and varied more strongly with applied voltage in the 0–0.4 V range than in the 0.4–0.8 V range.
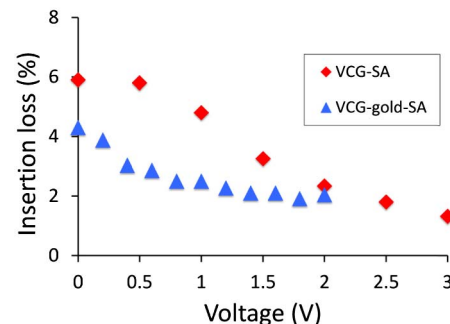

Fig. 4. (a) Power efficiency curves of the Cr:forsterite laser with the 4.7% output coupler in different cavity configurations. (b) Measured variation of the laser output power as a function of the bias voltage at a fixed input pump power of 7.15 W with the 2.4% output coupler.

Fig. 5. Measured single-pass insertion loss of the VCG-SA (two graphene electrodes) and VCG-gold-SA as functions of the bias voltage.
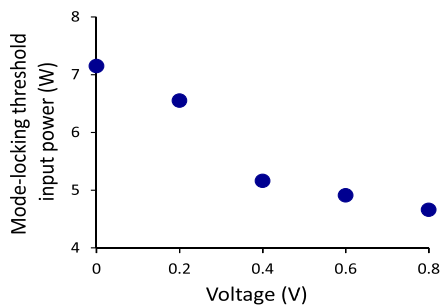
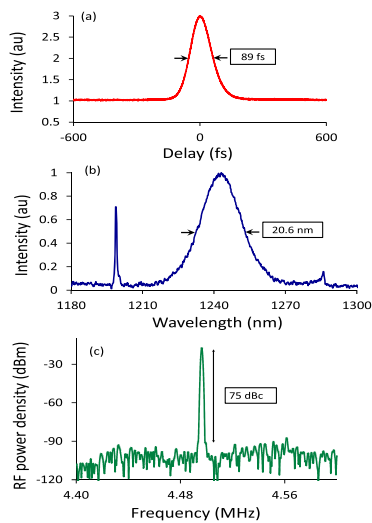**Fig. 6.** Measured threshold pump power for mode locking as a function of the applied bias voltage.

Fig. 7. (a) Intensity autocorrelation trace, (b) optical spectrum, and (c) RF spectrum at 1 kHz resolution bandwidth of the mode-locked pulses at the bias voltage of 0.4 V.

Figure 7 shows the mode-locking results obtained with the VCG-gold-SA at the bias voltage of 0.4 V The resonator produced 89 fs [Fig. 7(a)] nearly transform-limited pulses (time-bandwidth product = 0.35) with a peak power of 32 kW. Similar mode-locking results (pulse width = 80 fs, time-bandwidth product = 0.33, peak power = 42 kW) were obtained at 0.8 V. In both cases, Kelly sidebands were observed in the optical spectrum [see Fig. 7(b)] [17]. Figure 7(c) further shows that the sideband noise of the photodetected pulse train was 75 dBc (68 dBc at 0.8 V) below the fundamental tone of the RF (radio frequency) spectrum at the pulse repetition frequency of 4.51 MHz. These results further show that neither the applied voltage nor the supercapacitor design had a major effect on pulse characteristics. The VCG-gold-SA simply operates as a modulator to initiate mode locking, and the eventual pulse parameters depend mainly only on the resonator nonlinearities and dispersion.

At the highest single-pulse output power of 13 mW (15 mW), the maximum intracavity fluence on the VCG-gold-SA was estimated to be 290 μJ/cm^2 (335 μJ/cm^2) at 0.4 V

(0.8 V). No damage was observed on the sample at these fluence levels. Further output power increase resulted in pulsing instabilities and a continuous-wave spike appeared in the mode-locked spectrum. These instabilities arose because of insufficient dispersion to balance the cavity nonlinearities at higher intracavity energy levels.

In conclusion, we reported, for the first time to the best of our knowledge, use of a novel voltage controlled VCG-gold-SA for femtosecond pulse generation at 1.24 μm. The superior design of the VCG-gold-SA, in comparison with the previous design involving two graphene electrodes, enabled the operation of the laser with lower insertion loss and lower mode-locking threshold powers [13]. The VCG-gold-SA was successfully used inside a MPC Cr:forsterite laser to initiate the generation of transform-limited 89 fs (80 fs) pulses with a peak power of 32 kW (42 kW) at the bias voltage of 0.4 V (0.8 V). In comparison with conventional nanostructured carbon-based saturable absorbers, the supercapacitor architecture allows reversible, dynamic control of the absorption level. Furthermore, the high-dielectric electrolyte enables the control of absorption with low bias voltages on the order of a few volts. We foresee that the VCG-gold-SA has the potential to be implemented as a fast saturable absorber in a wide range of visible and near-infrared lasers.

REFERENCES

1. F. Bonaccorso, Z. Sun, T. Hasan, and A. C. Ferrari, Nat. Photonics **4**, 611 (2010).
2. K. S. Novoselov, V. I. Falko, L. Colombo, P. R. Gellert, M. G. Schwab, and K. Kim, Nature **490**, 192 (2012).
3. J. M. Dawlaty, S. Shivaraman, M. Chandrashekhar, F. Rana, and M. G. Spencer, Appl. Phys. Lett. **92**, 042116 (2008).
4. A. B. Kuzmenko, E. van Heumen, F. Carbone, and D. van der Marel, Phys. Rev. Lett. **100**, 117401 (2008).
5. I. H. Baek, H. W. Lee, S. Bae, B. H. Hong, Y. H. Ahn, D.-I. Yeom, and F. Rotermund, Appl. Phys. Express **5**, 032701 (2012).
6. M. N. Cizmeciyan, H. Cankaya, A. Kurt, and A. Sennaroglu, Appl. Phys. B **106**, 887 (2012).
7. Z. Sun, T. Hasan, and A. C. Ferrari, Physica E **44**, 1082 (2012).
8. C. C. Lee, S. Suzuki, W. Xie, and T. R. Schibli, Opt. Express **20**, 5264 (2012).
9. L. M. Malard, K. F. Mak, A. H. C. Neto, N. M. R. Peres, and T. F. Heinz, New J. Phys. **15**, 015009 (2013).
10. C. C. Lee, C. Mohr, J. Bethge, S. Suzuki, M. E. Fermann, I. Hartl, and T. R. Schibli, Opt. Lett. **37**, 3084 (2012).
11. R. M. Lynden-Bell, A. I. Frolov, and M. V. Fedorov, Phys. Chem. Chem. Phys. **14**, 2693 (2012).
12. E. O. Polat and C. Kocabas, Nano Lett. **13**, 5851 (2013).
13. I. Baylam, M. N. Cizmeciyan, S. Ozharar, E. O. Polat, C. Kocabas, and A. Sennaroglu, Opt. Lett. **39**, 5180 (2014).
14. J. Yan, Y. B. Zhang, P. Kim, and A. Pinczuk, Phys. Rev. Lett. **98**, 166802 (2007).
15. A. Sennaroglu, A. M. Kowalevicz, E. P. Ippen, and J. G. Fujimoto, IEEE J. Quantum Electron. **40**, 519 (2004).
16. S. Ozharar, I. Baylam, M. N. Cizmeciyan, O. Balci, E. Pince, C. Kocabas, and A. Sennaroglu, J. Opt. Soc. Am. B **30**, 1270 (2013).
17. S. M. J. Kelly, Electron. Lett. **28**, 806 (1992).